Supporting Information

On the Cobalt Carbide Formation in a Co/TiO_2 Fischer-Tropsch Synthesis Catalyst as Studied by High-Pressure, Long-Term Operando X-Ray Absorption Spectroscopy and Diffraction

Ilse K. van Ravenhorst[a,†], Adam S. Hoffman[a,#], Charlotte Vogt[a,†], Alexey Boubnov[,#,$], Nirmalendu Patra[#], Ramon Oord[†], Cem Akatay[¥], Florian Meirer[†], Simon R. Bare[*,#], Bert M. Weckhuysen[*,†]

† Inorganic Chemistry and Catalysis group, Debye Institute for Nanomaterials Science, Utrecht University, Universiteitsweg 99, 3584 CG Utrecht, the Netherlands.

Stanford Synchrotron Radiation Lightsource (SSRL), SLAC National Accelerator Laboratory, Menlo Park, California 94025, United States.

¥ Honeywell UOP, Des Plaines, Illinois 60016, United States.

a These authors contributed equally to this work.

Corresponding authors:

*B.M.Weckhuysen@uu.nl

*SRBare@slac.stanford.edu

Content

S1. Catalyst Characterization

S1.1 N_2-physisorption

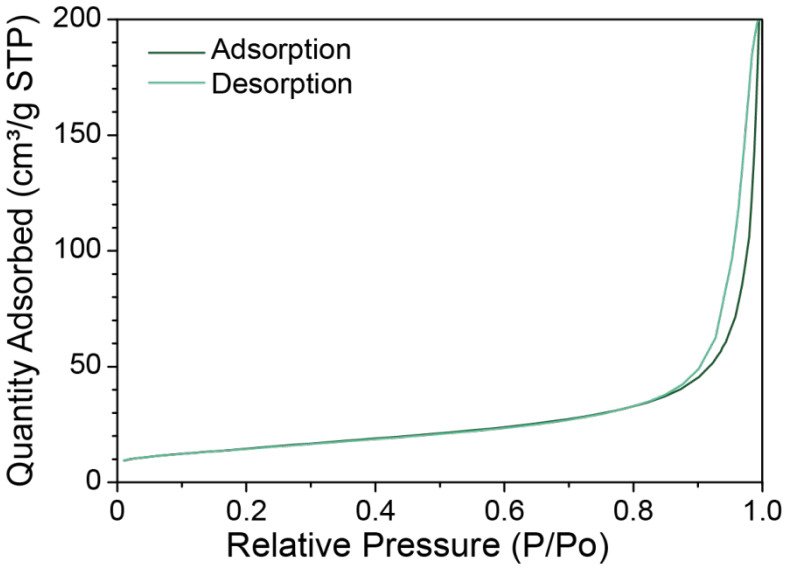

Figure S1. N_2-sorption curve of the support material (Titania, P25)

S1.2 X-ray Diffraction

Figure S2 shows the X-ray diffraction (XRD) pattern of the calcined (fresh, yellow line) and reduced

(grey line) 10 wt.% Co/TiO_2 catalyst diluted with diamond powder (microcrystalline powder, ~1 µm, Sigma Aldrich) in a ratio of 1:3 by mass. Phases of bulk compounds are represented by the stick plots below the diffractograms. The metallic cobalt is divided in two phases, Co-fcc (dark green and *) and Co-hcp (light green and o), and for clarity those sticks are shown with an offset. The diamond peaks are indicated with the ◊. From this pattern it is clear that the strongest metallic cobalt peaks overlap with the diamond peaks. Figure S3 shows the X-ray diffraction (XRD) pattern of the calcined (fresh, yellow line) and reduced (grey line) undiluted 10 wt.% Co/TiO_2 catalyst. Here the metallic cobalt peaks are visible for the reduced catalyst.

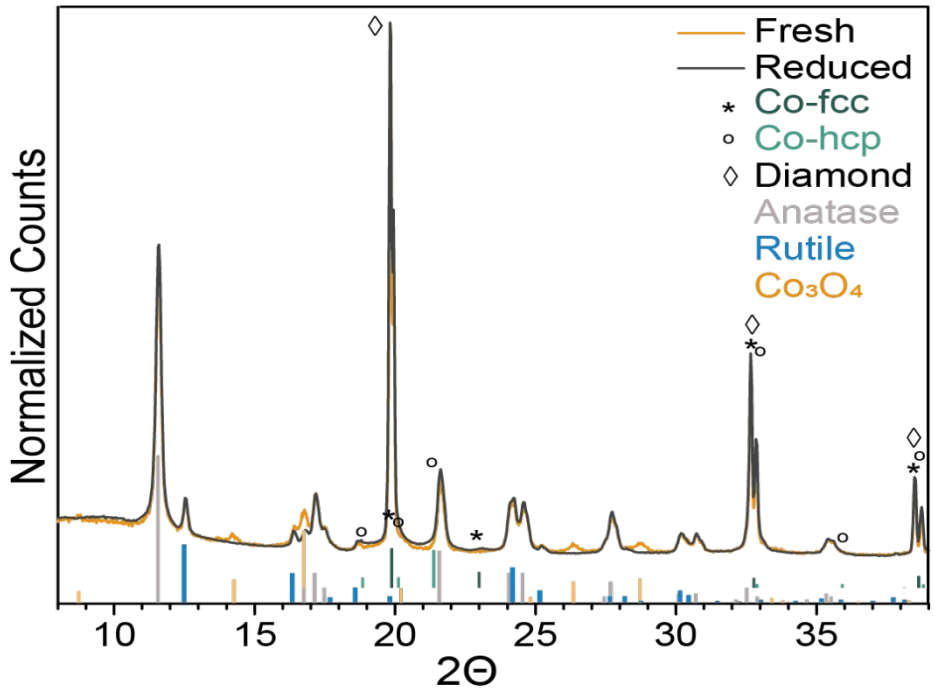

Figure S2. X-ray diffraction pattern of fresh and reduced ~10 wt.% $CoTiO_2$ catalyst diluted with diamond powder in a ratio of 1:3 by mass

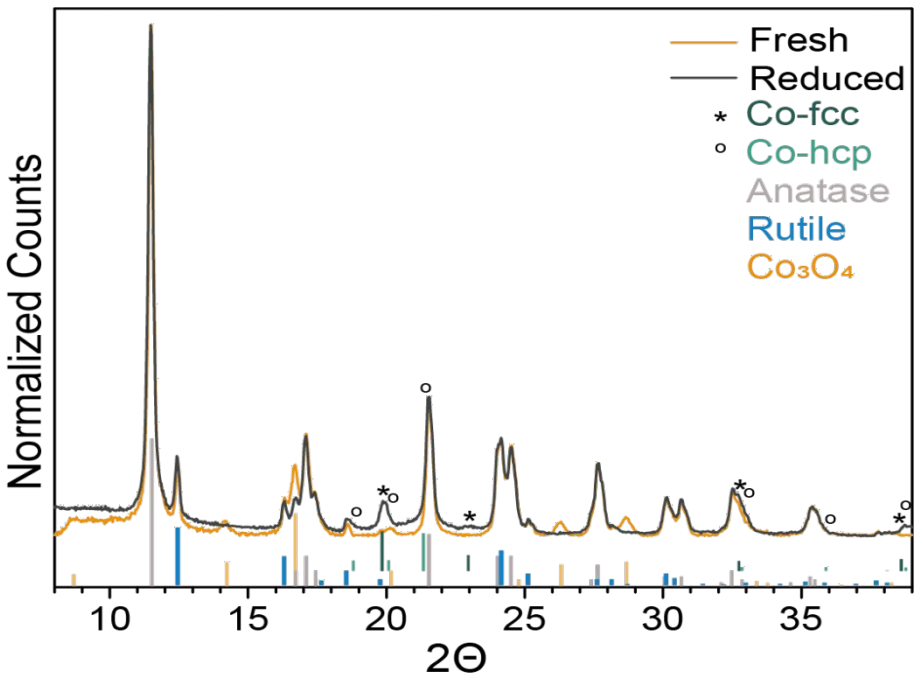

Figure S3 X-ray diffraction pattern of fresh and reduced ~10 wt.% $CoTiO_2$ catalyst.

S1.3 HAADF-STEM-EDX mapping Co/Ti ratio

Table S1 Co/Ti ratio of fresh catalyst determined from EDX in the STEM for several regions. The average ratio was

	Co/Ti
Region 1	0.10
Region 2	0.09
Region 3	0.05
Region 4	0.10
Region 5	0.10
Region 6	0.13
Region 7	0.12
Region 8	0.12
Average	**0.10**
St. Dev	0.025
St. Err	0.009

S1.4 Reduction: XRD and XAS

Reduction of the ~10 wt.% Co/TiO_2 diluted with diamond dust is shown in Figure S4 and S5 for XRD and XAS, respectively. In both cases, the temperature was increased to 400 °C in pure H_2 (10 °C/min) at atmospheric pressure and was held at temperature for 2 h. The reduction follows two steps. In the first reduction step Co_3O_4 species are reduced to CoO. The second step follows after Co_3O_4 is depleted and represents the reduction of CoO to metallic Co.

In the inset of Figure S4, the intensity sticks of different cobalt phases are indicated to show the two-step pathway. The peaks representing Co_3O_4 (yellow sticks) disappear and the CoO peaks are coming up (red sticks). The latter disappear as well as the metallic cobalt peaks arise (dark and light green sticks). From analysis by Rietveld refinement in the Brucker TOPAS software, the averaged particle size was calculated at 15-20 nm. This same pathway from Co_3O_4 to CoO and metallic Co is clearly visible in Figure S5 for the XAS experiment. Due to unforeseen circumstances at the beamline, the reduction had to be performed twice (partially), prior the Fischer-Tropsch synthesis. Figure S5a shows the linear combination fitting done in the Athena software, making use of the fresh catalyst (representing the Co_3O_4 phase), a CoO reference and a metallic cobalt foil reference, where panel Figure S5b shows the XANES spectra during reduction. Figure S6 shows both reductions. It can be seen that the catalyst only re-oxidized to CoO after exposure to air and was easily reduced again.

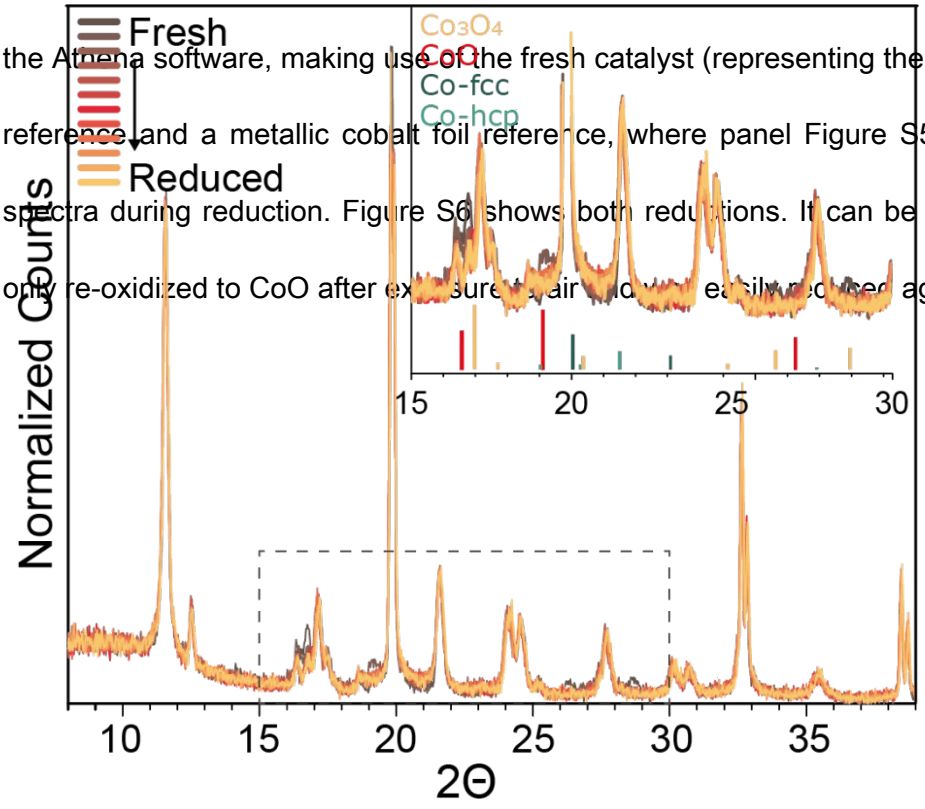

Figure S4 *In situ* X-ray diffraction patterns of the reduction (at 400 °C for 2 h with 3 mL/min pure H_2) of the ~10 wt.% Co/TiO_2 diluted 1:3 with diamond powder by mass. The two-step pathway from Co_3O_4 to CoO to metallic Co is clearly visible. The inset

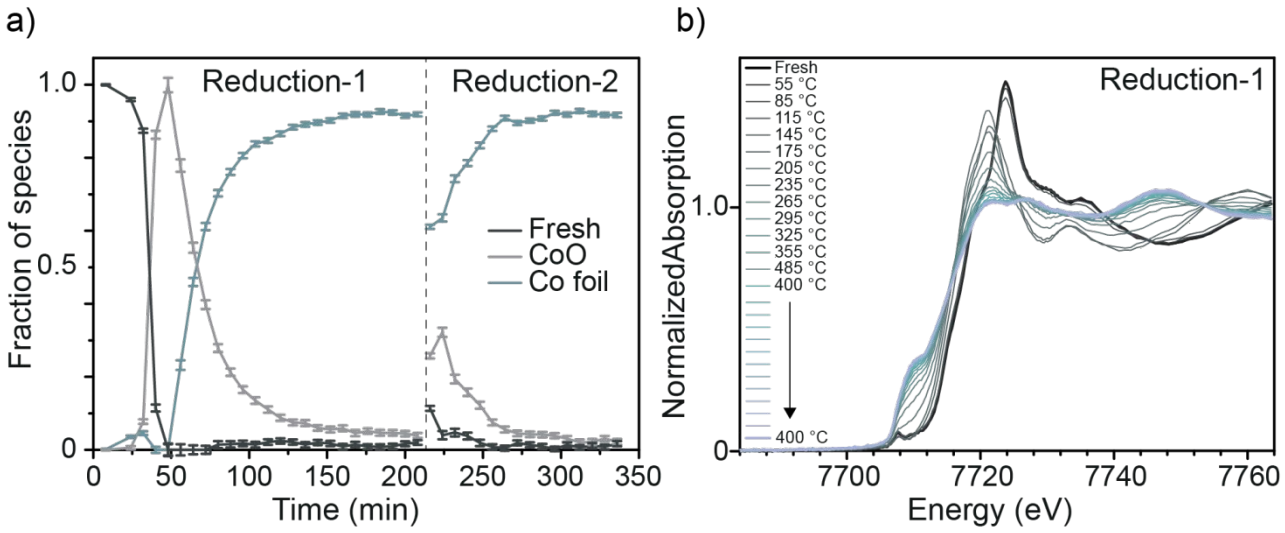

Figure S5 a) The two step pathway from Co_3O_4 to CoO to metallic Co is clearly visible, when a linear combination fitting is done using the spectrum of the fresh catalyst (as Co_3O_4), a CoO reference and a metallic Co foil reference (Co-fcc). Due to unforeseen circumstances the catalyst was exposed to air and a second reduction was done prior FTS, indicated by the dashed line. b) *In situ* X-ray absorption spectra of the first reduction (at 400 °C with 5 mL·min^{-1}

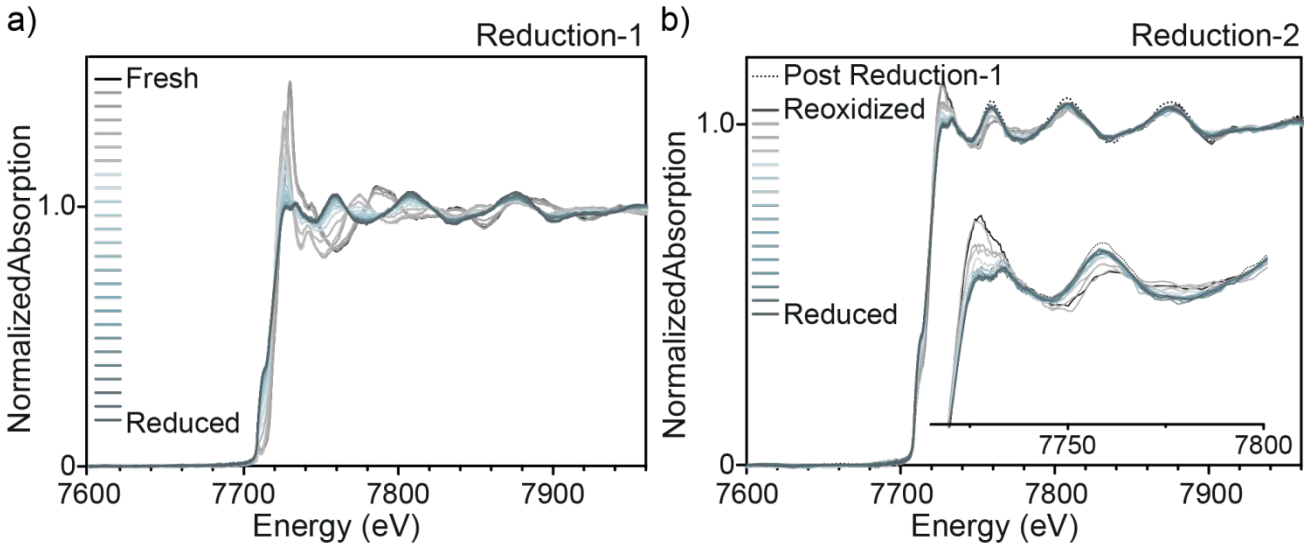

Figure S6 a) Shows the first reduction and b) the second, after unforeseen circumstances prior the Fischer-Tropsch synthesis. As can be seen, the catalyst only re-oxidized to CoO and was easily reduced again.

S1.5 Catalytic Testing

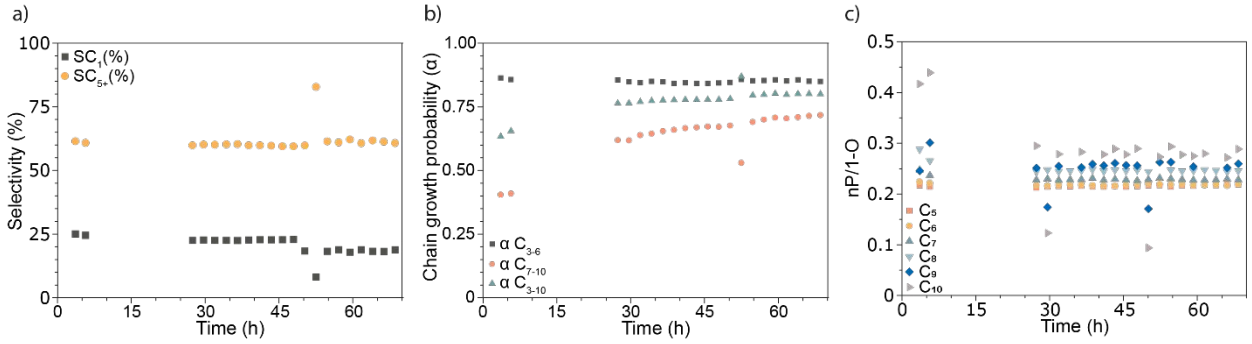

Figure S7 Catalytic testing done by Shell Global Solution B.V., Amsterdam. a) shows the selectivity towards C_1 (methane) and C_{5+} during a 60+ h catalytic run at 220 °C, 13 bar and a H_2/CO ratio of 1. b) shows the numbers for different selected hydrocarbon regions within the run. c) Represents the n-paraffin/ 1-olefin ratio for the hydrocarbons $C_{5\text{-}10}$.

S2 Extra Information on the Undiluted XRD Experiment

S2.1 Mass Spectrometry of the undiluted XRD experiment

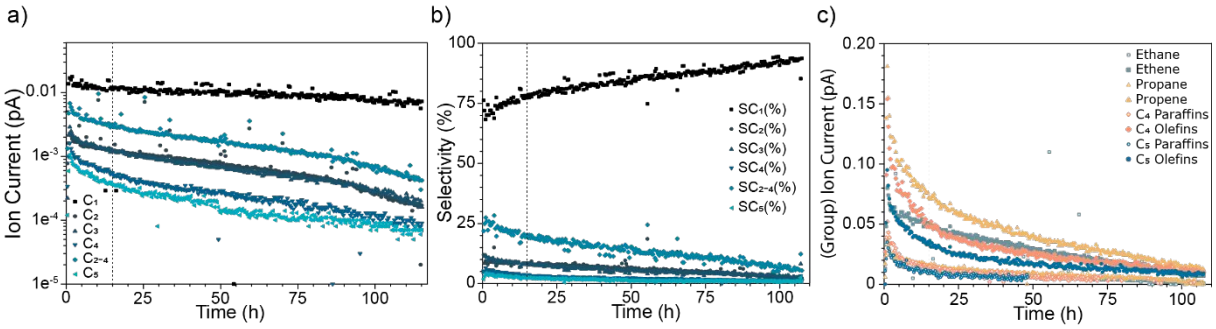

Figure S8 *Operando* activity of the undiluted 10 wt.% Co/TiO_2 catalyst, as measured by gas chromatography (GC) during a 120 h experiment while simultaneously measuring XRD. The grey dotted line in each panel indicates the start of carbide formation as determined by XRD. a) The sum of the different products formed from C_1 to C_5. b) The selectivity towards those different products showing a preference towards methane. c) Comparison of the production of olefins and paraffins. Note that C_5 products were not quantified in this experiment.

S3. Extra information on Operando X-ray Absorption Spectroscopy

S3.1 Experimental procedure for first operando XAS experiment

The length of the catalyst bed was approximately 5 mm. The capillary was loaded in to a custom built *operando* XAS cell.[1] A graphite ferrule was used to hold a thermocouple in place in the gas stream, fed into the quartz capillary, pressed against the quartz wool ensuring correct temperature measurement and catalyst bed stability. The flow system was leaked checked with helium at 15 bar prior to the start of the experiment. The cobalt in the catalyst was reduced at ambient pressure at 400°C under a flow of 50% H_2, balance helium, at a flow

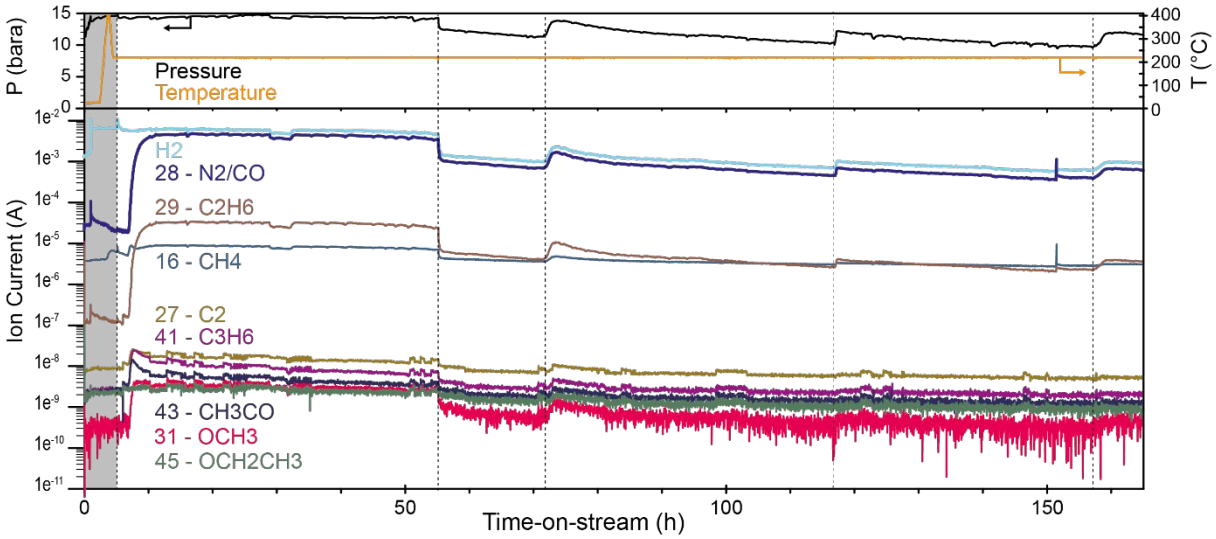

Figure S9. Mass spectrometry results and the pressure (black line) and temperature (yellow line) profile for the 6-day XAS experiment. The grey area shows the reduction period at 400 °C. As soon as Fisher-Tropsch conditions start at 220 °C, products are forming and stay fairly stable over time with the exception of the changes due to the pressure changes (indicated by the dashes lines). After 50 h time-on-stream the pressure

rate of 3 ml·min^{-1} with a ramp rate of 10 °C·min^{-1}. The cell was then cooled to 220°C and pressurized to 14 bar in a 1:1 H_2:CO at a total flow rate of 3 ml·min^{-1}. A mass spectrometer (Hiden Analytical QGA) was used to determine and quantify reaction products on-line in the gas stream during the XAS experiments (Figure S8).

S3.2 Mass Spectrometry of the Second XAS Experiment

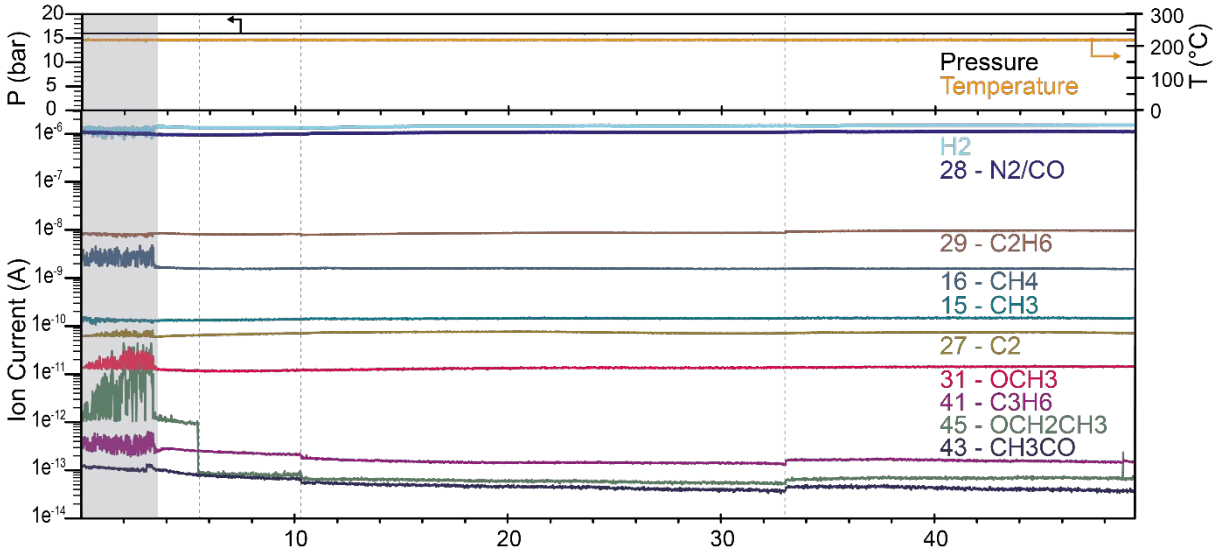

Figure S10. Mass spectrometry results for the 48 h XAS experiment. The grey area shows a stabilization period after which the products stay stable with time-on-stream (TOS). The upper part shows stable temperature and pressure with TOS. Dotted lines indicate sudden product jumps without a known reason.

S3.3 X-ray Absorption Spectroscopy Analysis Procedures

S3.3.1 Co references and modeling of Co-fcc

Figure S11 shows the Co K-edge XANES of for Co_3O_4, CoO, Co-hcp, Co-fcc and Co_2C

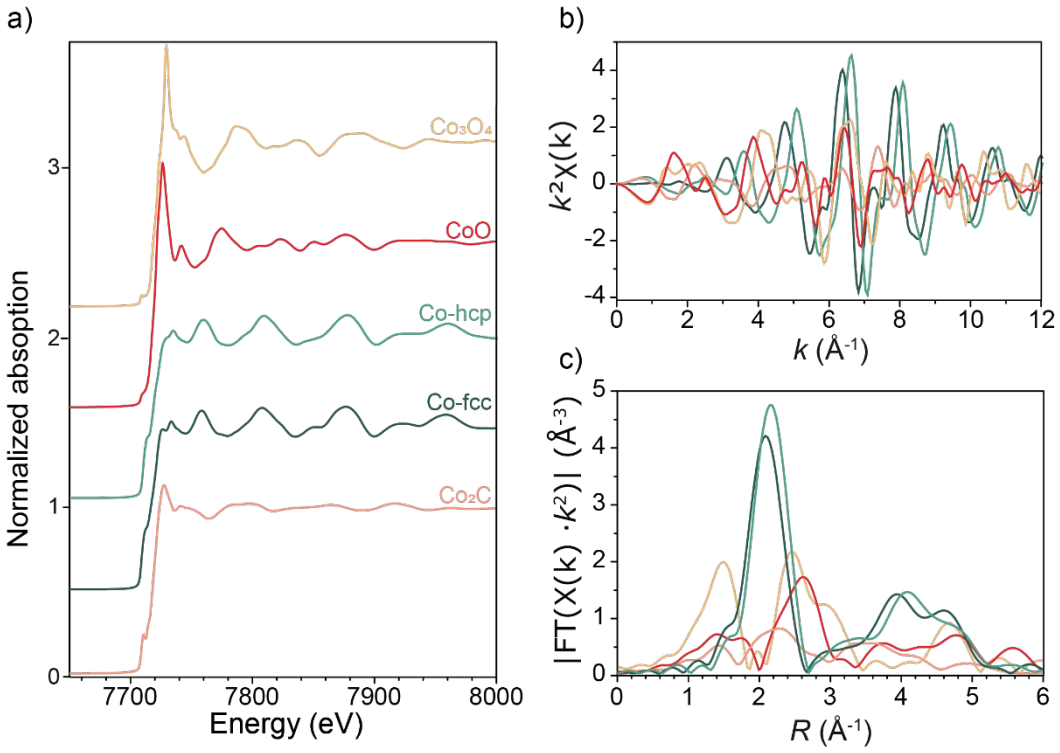

Figure S11. Reference spectra for Co_3O_4, CoO, Co-fcc, Co-hcp and Co_2C. XANES are shown in a (top to bottom, offset for clarity), *k* and *R* space in b and c, respectively.

references, as well as *k* and *R* space, used in this manuscript.

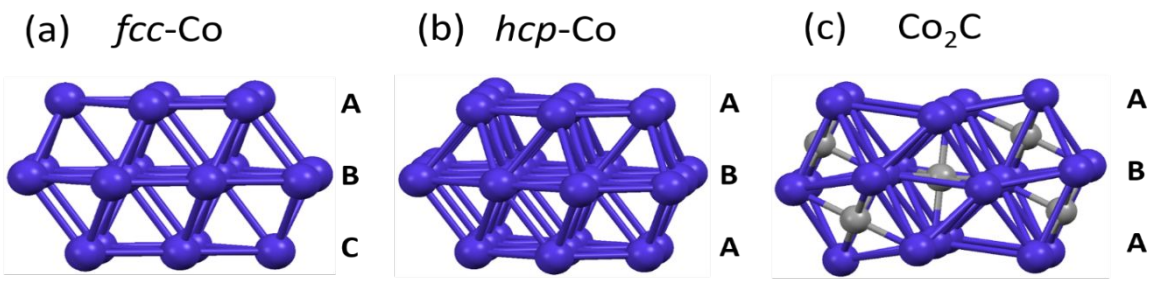

Figure S12. A view of the phases (a) *fcc*-Co, (b) *hcp*-Co and (c) Co_2C to demonstrate the similarity of their metal lattice. The Co_2C phase is formed by carbon insertion into the *hcp*-Co phase with a corresponding

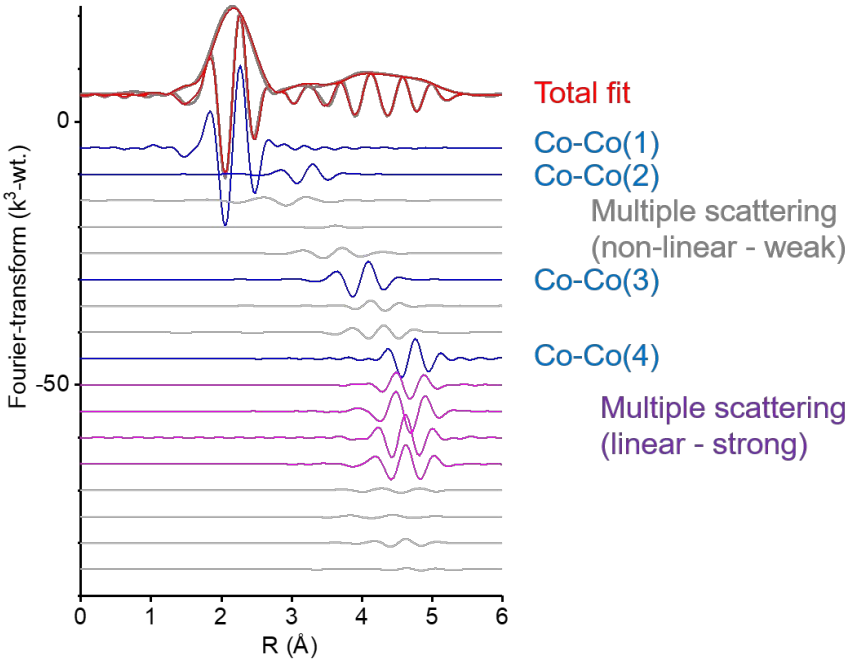

Figure S13. EXAFS fit of Co foil using the *fcc*-Co model, displaying the imaginary part of all contributing single-scattering and multiple-scattering paths. Only the strongest paths up to 5.0 Å are displayed. Table S2 lists all the paths

Table S2: EXAFS refinement of Co foil EXAFS in Figure S13 with analogous color-coding: blue, single-scattering; grey, non-linear multiple-scattering (MS) and purple, linear MS. The spectrum was refined in k-range 3.0-14.3 $Å^{-1}$ and R-range 1.0-5.5 Å; maximum number of parameters was $N_{Nyquist}$ = 32, of which 16 were refined.

Shared fitting parameters: [a-h] interatomic distances (d), [i-n] mean squared displacement (σ^2).

Sample	Path	d [Å]	CN (fixed)	σ^2 [$Å^2$]	ΔE_0 [eV]	R-factor [%]
***fcc*-Co**	Co-Co(1)	2.50 ± 0.00	12	0.006 ± 0.000	-4.6 ± 0.6	1.0
	Co-Co(2)	3.53 ± 0.01	6	0.010 ± 0.002		
	Triangular MS	3.75 ± 0.01	48	0.010 ± 0.004[i]		
		4.26 ± 0.01[a]	24	0.010 ± 0.004[i]		
		4.26 ± 0.01[a]	48	0.010 ± 0.004[i]		
	Co-Co(3)	4.33 ± 0.01	24	0.009 ± 0.001		
	Triangular MS	4.66 ± 0.01[b]	48	0.005 ± 0.003[j]		
		4.66 ± 0.01[b]	96	0.005 ± 0.003[j]		
	Co-Co(4)	5.00 ± 0.01	12	0.017 ± 0.043		
	Non-forward lin. MS	5.00 ± 0.01[c]	12	0.022 ± 0.051		
	Forward-lin. MS	5.00 ± 0.01[c]	24	0.010 ± 0.003		
	Fwrd through abs. MS	5.00 ± 0.01[c]	12	0.022 ± 0.051		
	Double-fwrd. MS	5.00 ± 0.01[c]	12	0.010 ± 0.003		
	Hinge MS	5.00 ± 0.01[d]	48	0.000 ± 0.003[k]		
	Dog-leg MS	5.00 ± 0.01[d]	48	0.000 ± 0.003[k]		
	Rattle MS	5.00 ± 0.01[d]	12	0.000 ± 0.003[k]		
	Dog-leg MS	5.00 ± 0.01[d]	48	0.000 ± 0.003[k]		
	Triangular MS	5.18 ± 0.01[e]	48	0.007 ± 0.016[l]		
		5.18 ± 0.01[e]	48	0.007 ± 0.016[l]		
		5.58 ± 0.01[f]	96	0.007 ± 0.016[l]		
		5.58 ± 0.01[f]	48	0.007 ± 0.016[l]		
	Co-Co(5)	5.59 ± 0.01	24	0.016 ± 0.009		
	Triangular MS	5.81 ± 0.01[g]	48	0.030 ± 0.060[m]		
		5.81 ± 0.01[g]	48	0.030 ± 0.060[m]		
		5.81 ± 0.01[g]	48	0.030 ± 0.060[m]		
		5.91 ± 0.01[h]	96	0.030 ± 0.060[m]		
		5.91 ± 0.01[h]	96	0.030 ± 0.060[m]		
	Triple MS	5.91 ± 0.01[h]	96	0.017 ± 0.015[n]		
		5.91 ± 0.01[h]	96	0.017 ± 0.015[n]		

S3.3.2 k^2 space during FTS and modelling

k space during the 47 h FTS experiment. Figure 14a shows everything during the experiment, while b represents the modelling (described below) of the start and the end of FTS, as well as

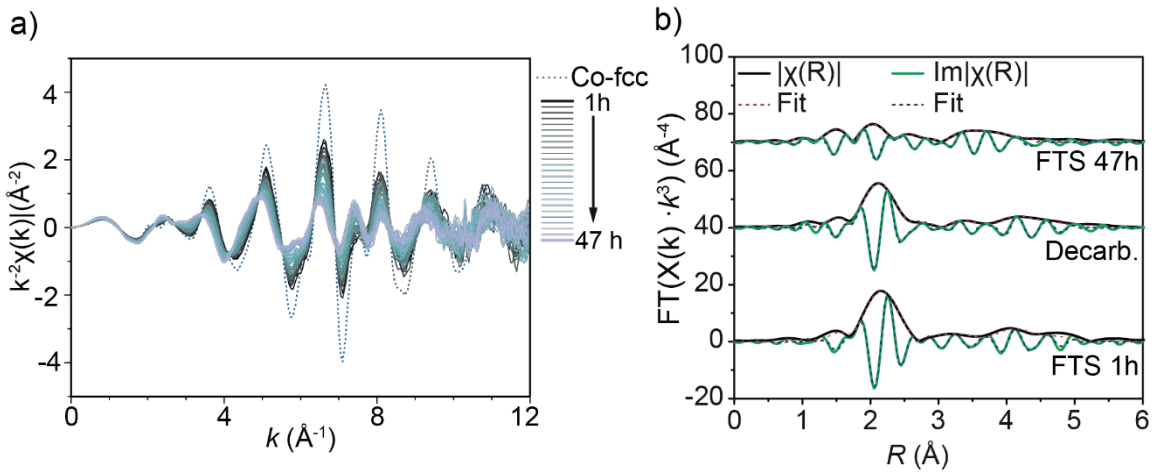

Figure S14. a) The EXAFS data in *k*-space during the 47 h FTS experiment together with a Co reference. b) k space for only the beginning and end state of the FTS run with modeling, as well as after decarburization. Solid

after decarburization.

S3.3.3 Modeling of first, last and decarburized sample

Prior to the XAFS data analysis the initial treatment of the experimentally obtained raw data was conducted using the Athena software following the standard procedure. Spectra were energy calibrated (using the Co foil that was simultaneously scanned during the experiment), merged, and normalized.

The first scan under FTS and the decarburized sample at 300°C have similar XANES feature, the last scan during FTS has different curve shapes from the reference metal just above the absorption edge indicating a different atomic environment around the Co atoms. The absorption features above the edge of the spectra at 47 h FTS are quite similar to the spectra as reported earlier for the pure Co_2C as synthesized sample [2,3] However, a lesser white line

intensity of the last scan sample can indicate towards an incomplete formation of perfect Co_2C phase or the add mixture of secondary metallic Co phase.

Following the standard data treatment procedures in Athena interface the energy dependent absorption spectra were converted to *k* space and later the k^3 weighted $\chi(k)$ spectra were Fourier transformed to *R* space ($\chi(R)$). EXAFS modelling was done over the *k* range 3.0 – 11.7 $Å^{-1}$ and a *R* range 1.3 – 4.3 Å. The Artemis software was used for modelling the data using IFEFFIT software package. A comparison between the k^3 weighted $\chi(k)$ and phase corrected FT-EXAFS spectra ($\chi(R)$) of the Co catalysts are shown in the Figure S14b and S15a. When modelling the EXAFS, scattering paths were simulated from Co-hcp metal (mp-54, P63/mmc; a = b = 2.50Å, c = 4.03Å) and Co_2C (mp-22488, Pnnm; a = 2.90Å, b = 4.45Å, c = 4.37Å) using feff6 in the Artemis software. The rational for using Co-hcp vs. Co-fcc is discussed below.

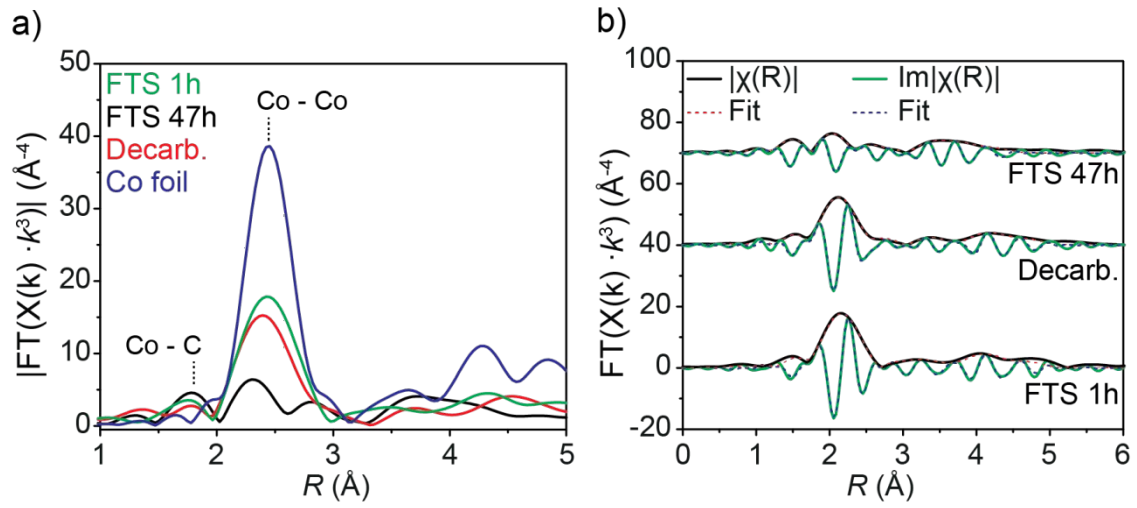

Figure S15. a) Comparison between the Fourier Transformed EXAFS spectra (($\chi(R)$ vs *R*)) of the samples along with the Co-hcp foil. b) The magnitude and imaginary components of the EXAFS data and best-fit models of

From the structural point of view, it is difficult to discriminate between the Co-hcp and Co-fcc phases by EXAFS modelling as both structures have similar Co – Co atomic arrangements in the 1st and 2nd coordination shells (Figure S12 and Table S3). The 3rd coordination shell of the Co-hcp phase has lesser intensity compared to Co-fcc phase because of lesser C.N and in the

4th co-ordination shell of Co-fcc has higher intensity because of multiple scattering paths.[3,4] When using cif files to generate scattering paths, the cif file for Co-hcp was used instead of Co-fcc as the linear combination fitting results showed that the majority (~ 80%) of Co-hcp phase present in the First scan and Decarburized catalysts. Attempts to model the data using Co-fcc structure files were also done, but the overall R-factor was worse for each model. This suggests, but is not conclusively proven, that the Co phase present under FTS conditions and after decarburization is Co-hcp instead of Co-fcc.

Inspection of the EXAFS spectra at the start of FTS and after decarburization show a mostly metallic Co phase with a scattering component observed at approximately at 2.5 Å, but the presence of a scattering component at 1.9 Å indicates carbide formation during FTS and residual carbide after decarburization This path was modelled as the Co–C scattering path from Co_2C in all the samples, discussed further below. The spectral shape of the FT-EXAFS spectra of the 47 h FTS scan matches to the previously reported results which shows that Co reacts with syngas forming a mixed phase of Co_2C and metallic Co.[3,5]

Depending upon the quantity of the mixed phases the coordination number of the above mentioned scattering paths varies with reaction conditions. This has been quantified here in details. The values of the EXAFS best fitted parameters for the First scan, Decarburized and Last Scan samples are summarized in Tables S4-6, respectively.

Modelling of the EXAFS data was an iterative process. Given the strong scattering path at 2.5 Å in the FTS 1 hr and decarburized scans the two spectra were modelled with only scattering

paths from Co-hcp. Likewise, the similarity of the FTS 47 h scan to that of bulk Co_2C initially resulted in a model containing scattering paths from Co_2C. These models were able to account for some features in the EXAFS but not all of them. The inclusion of a second phase (either Co_2C or Co-hcp) was required to obtain the best fit models as observed by the improvement of the quality of the data fitting or minimizing the mismatch between the experimental data and theoretically generated spectra as well as an improvement in the error of the models.

To model the mixed phase EXAFS simultaneous fitting, with shared parameters, was performed. The FT-EXAFS spectra and their imaginary parts fitted with the corresponding theoretically generated model are depicted in the Figure S15b. In addition to this, a rough estimation about the phase fraction of the metallic Co and Co_2C was obtained from the data fitting by multiplying the bulk coordination of each scattering paths to a phase factor **x** for Co_2C and **(1-x)** for metallic Co. The phase fraction between the Co_2C and metallic Co phases were obtained near to 60:40 ratios.

The coordination number of the Co – C scattering path for the FTS 1 h and Decarburized scans is less than 1 while it is near to 2 for the FTS 47h scan, indicating a lesser Co carbide fraction during the beginning of FTS and after decarburization compared to 47 h of FTS. The value of Co – C coordination number and atom to atom distances match to the previously reported results for freshly carburized catalysts.[5] The value of the Co – Co coordination number in the 1st Co-CO scattering path is close to the bulk coordination and much higher for the FTS 1 h and decarburized scans than the FTS 47 h scan indicating a dominant metallic Co present in these samples. The scattering paths at longer R distances have reduced coordination numbers in comparison to the bulk materials possibly as a result of particle size effect of the nanoparticles.

As a conclusion, the work shows that Co_2C scattering paths can be detected in the first hour of FTS and that the Co nanoparticles are partially converted to cobalt carbide during the 47 h FTS experiment. Decarburization at 300°C converts the majority of the carbide phase back to metallic Co, though there is some residual carbide present.

Table S3. EXAFS best fitted structural parameters values for them Co-hcp and fcc references

Sample	Path	E_0 (eV)	S_0^2	R (Å)	σ^2(Å^2)	R *factor*
Co-hcp	Co – Co (12)	8.18 ± 0.04	**0.79 ± 0.03**	2.50 ± 0.01	0.006 ± 0.001	0.006
	Co – Co (6)			3.50 ± 0.01	0.011 ± 0.002	
	Co – Co (18)			4.36 ± 0.007	0.008 ± 0.001	
Co-fcc	Co – Co (12)	8.25 ± 0.59	0.77 ± 0.05	2.50 ± 0.01	0.006 ± 0.001	0.010
	Co – Co (6)			3.54 ± 0.02	0.011 ± 0.002	
	Co – Co (24)			4.34± 0.01	0.009 ± 0.001	

Table S4. EXAFS best fitted structural parameters values for First Scan sample using Co-hcp and Co_2C as fitting models.

Phase	Path	E_0 (eV)	C.N	R (Å)	σ^2(Å^2)	R *factor*
Co_2C	Co – C (3)	9.08 0.28	**0.63** ± 0.06	1.92 ± 0.03	0.002 ± 0.001	0.011
	Co – Co (5)		1.13 ± 0.06	2.69 ± 0.01	0.002 ± 0.001	
	Co – Co (4)		1.19 ± 0.06	2.80 ± 0.01	0.002 ± 0.001	

	Co – Co (2)		0.52 ± 0.16	2.94 ± 0.01	0.002 ± 0.001	
	Co – C (1)		0.58 ± 0.35	3.17 0.05	0.002 ± 0.001	
Co	Co – Co (12)	9.82 0.23	11.85 ± 0.04	2.51 ± 0.01	0.011 ± 0.001	
	Co – Co (6)		4.57 ± 0.10	3.52 ± 0.02	0.011 ± 0.001	
	Co – Co (18)		10.85 ± 0.06	4.38 ± 0.01	0.011 ± 0.001	
	Co – Co (12)		8.59 ± 0.15	4.87 ± 0.02	0.011 ± 0.001	

Table S5. EXAFS best fitted structural parameters values for Last Scan sample using Co-hcp and Co_2C as fitting models.

Phase	Path	E_0 (eV)	C.N	R (Å)	σ^2(Å^2)	R *factor*
Co_2C	Co – C (3)	9.37 ± 0.49	**1.72** ± 0.03	1.90 ± 0.01	0.002 ± 0.001	0.016
	Co – Co (5)		3.12 ± 0.03	2.71 ± 0.01	0.002 ± 0.001	
	Co – Co (4)		2.22 ± 0.05	2.82 ± 0.01	0.002 ± 0.001	
	Co – Co (2)		1.46 ± 0.11	2.96 ± 0.01	0.002 ± 0.001	
	Co – C (1)		0.92 ± 0.08	3.14 ± 0.04	0.002 ± 0.001	
	Co – C (2)		1.98 ± 0.10	3.46 ± 0.03	0.002 ± 0.001	
	Co – Co (3)		1.99 ± 0.07	3.95 ± 0.01	0.002 ± 0.001	
Co	Co – Co (12)	9.73 ± 0.23	7.53 ± 0.02	2.55 ± 0.01	0.010 ± 0.001	
	Co – Co (6)		3.16 ± 0.05	3.59 ± 0.01	0.010 ± 0.001	

	Co – Co (18)	6.40 ± 0.04	4.40 ± 0.01	0.010 ± 0.001	
	Co – Co (12)	1.98 ± 0.08	4.75 ± 0.03	0.010 ± 0.001	

Table S6. EXAFS best fitted structural parameters values for Decarburized sample using Co-hcp and Co_2C as fitting models.

Phase	Path	E_0 (eV)	C.N	R (Å)	σ^2(Å^2)	R_{factor}
Co_2C	Co – C (3)	9.32 0.28	**0.70** ± 0.04	1.92 ± 0.01	0.002 ± 0.001	0.017
	Co – Co (5)		2.28 ± 0.05	2.71 ± 0.01	0.002 ± 0.001	
	Co – Co (4)		1.19 ± 0.06	2.82 ± 0.01	0.002 ± 0.001	
	Co – Co (2)		1.32 ± 0.10	2.96 ± 0.01	0.002 ± 0.001	
	Co – C (1)		0.58 ± 0.40	3.15 ± 0.05	0.002 ± 0.001	
Co	Co – Co (12)	9.86 0.23	11.01 ± 0.03	2.52 ± 0.01	0.010 ± 0.001	
	Co – Co (6)		3.04 ± 0.09	3.55 ± 0.02	0.010 ± 0.001	
	Co – Co (18)		11.57 ± 0.06	4.40 ± 0.01	0.010 ± 0.001	
	Co – Co (12)		8.11 ± 0.11	4.86 ± 0.02	0.010 ± 0.001	

S3.3.4 PCA and clustering

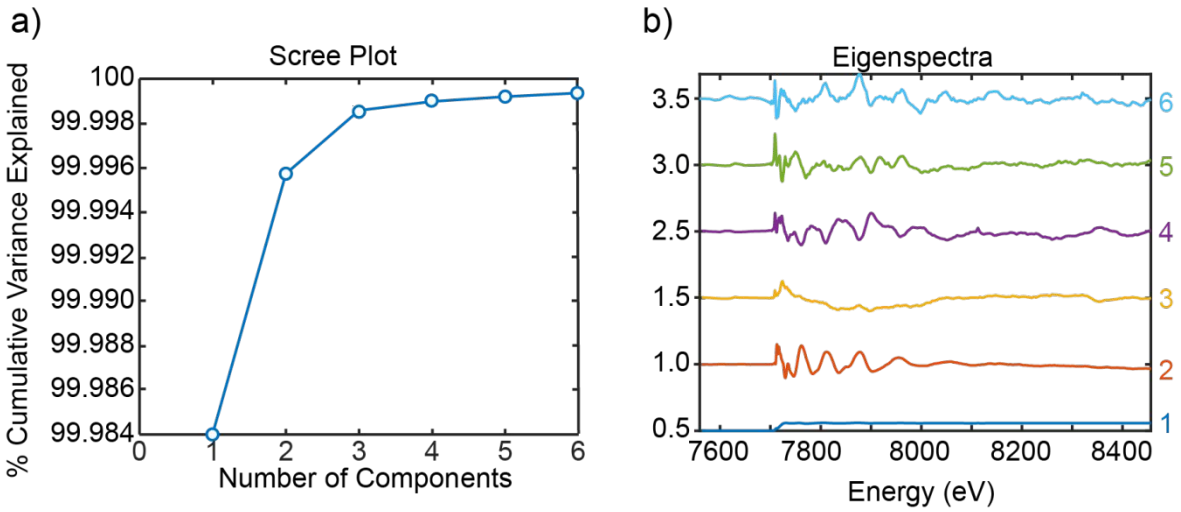

Figure S16 a) Scree plot of the first 6 components from PCA and the eigenspectral of those components are shown in b).

S3.4 Extra information on the whole range linear combination fitting

LSLC is performed over a range of -20 to +50 eV around the absorption edge on the normalized spectra. The reference spectra where weighted between 0 and 1 but not forced to sum to 1. No noise was added and combinatorics was set to use all the selected references (Co-fcc, Co-hcp and Co_2C in case of FTS conditions and Co_3O_4, CoO, Co-fcc and Co-hcp in case of reduction conditions).

Figures S17-19 show the linear combination fitting of the whole range during FTS, with different combinations of references. When CoO is introduced, the error within TOS increases significant. When fitting with only a combination of Co-hcp or Co-fcc with Co_2C, there is not

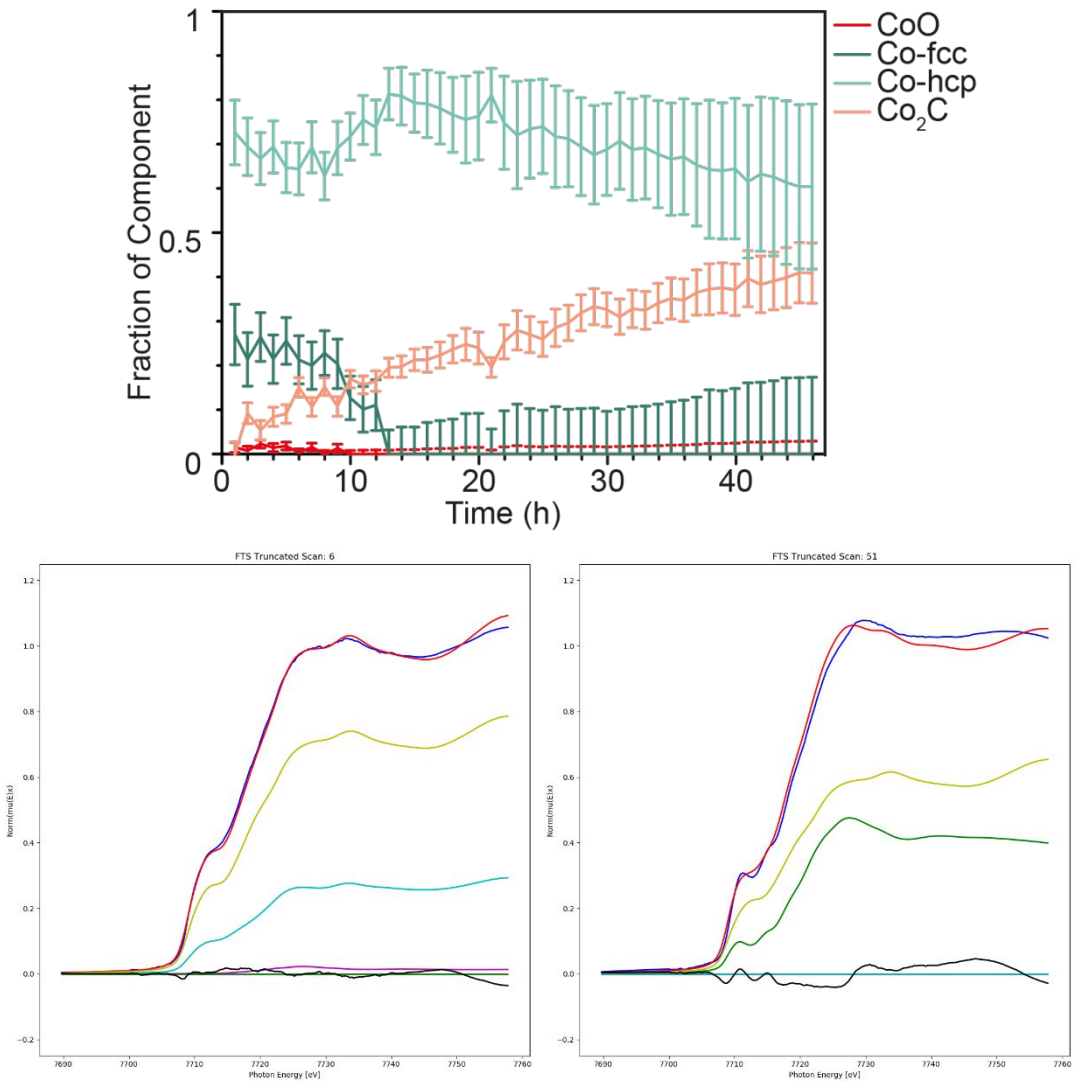

Figure S17. Top) Linear combination fitting of the whole FTS range with CoO, Co-fcc, Co-hcp and Co_2C references. Bottom) screen shots of the first and last scan fitting within Athena, respectively.

much difference. Screenshots of the first and last scan are included to show the misfit, especially at the end of FTS, which is most probably due to the nanoparticle effect and an intergrowth between the different phases of cobalt.

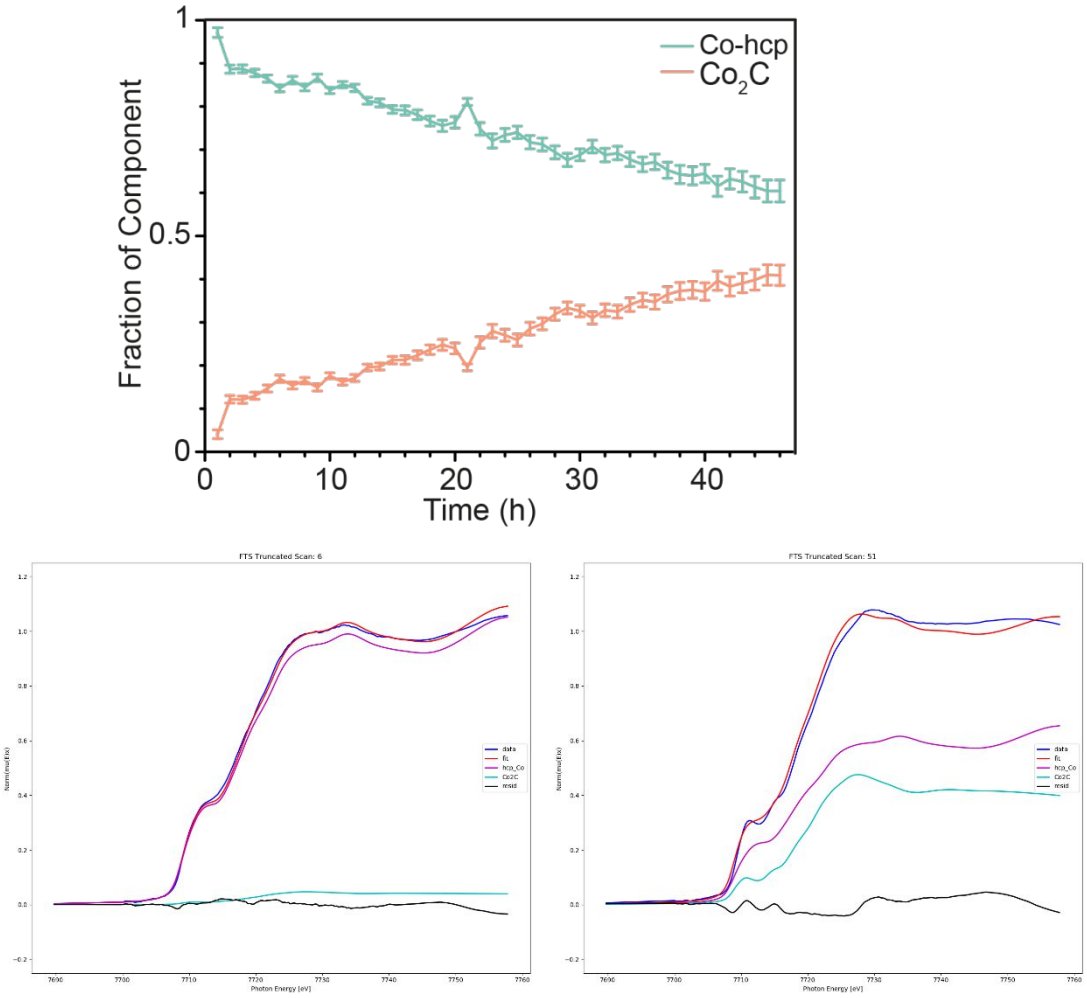

Figure S18. Top) Linear combination fitting of the whole FTS range with Co-hcp and Co_2C references. Bottom) screen shots of the first and last scan fitting within Athena, respectively

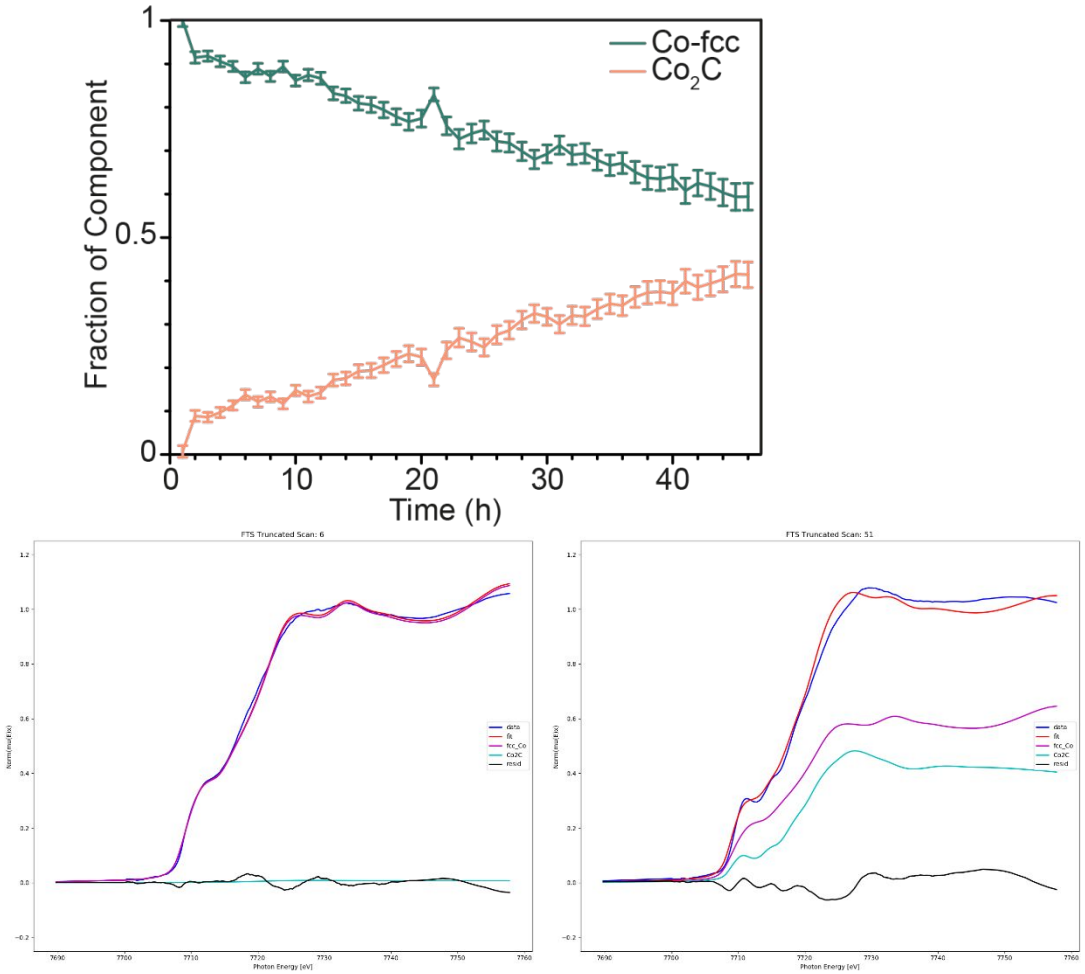

Figure S19. Top) Linear combination fitting of the whole FTS range with Co-fcc and Co_2C references. Bottom) screen shots of the first and last scan fitting within Athena, respectively

S3.5 Cauchy wavelet transform analysis

Continuous Cauchy wavelet transform (CCWT)[7] was used to visualize the changes in k- and R-space during the in-situ XAS FTS experiment. The CCWT was performed using a k-range

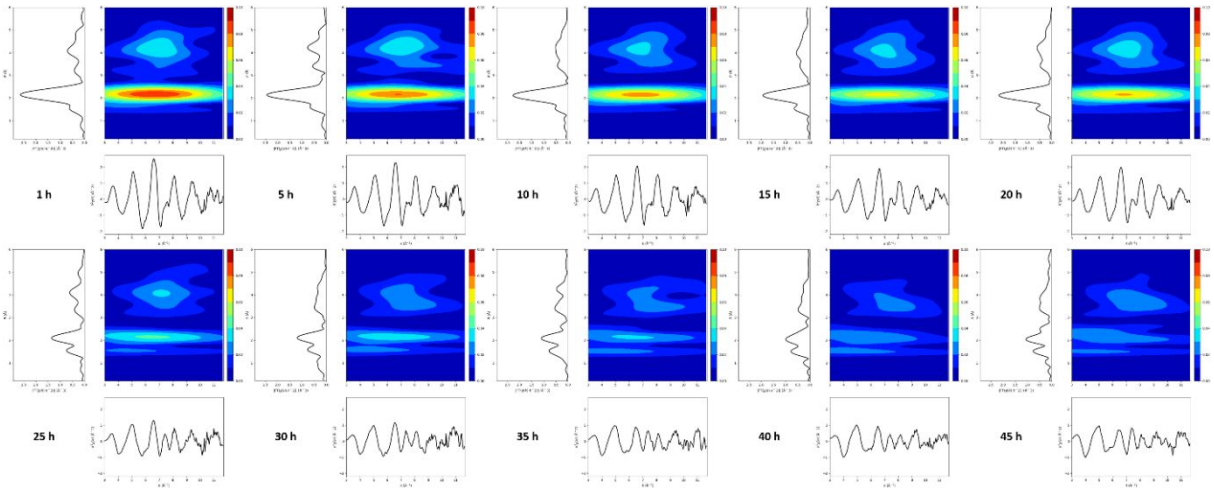

Figure S20. Continuous Cauchy wavelet transforms, consisting of k^2-weighted EXAFS, magnitude of the Fourier transform, and magnitude of the wavelet transform, of the EXAFS data shown in Figure 5 for every 5 h. The heat-map of the CCWT has been normalized to the largest and smallest values of all wavelet transforms for

of k = 0-11.7 Å and a R-range of R = 0.-6 for all EXAFS spectra.

S4 Potential cobalt oxide formation

The vertical bars indicate where the relevant diffraction peaks would occur for several relevant materials or material phases

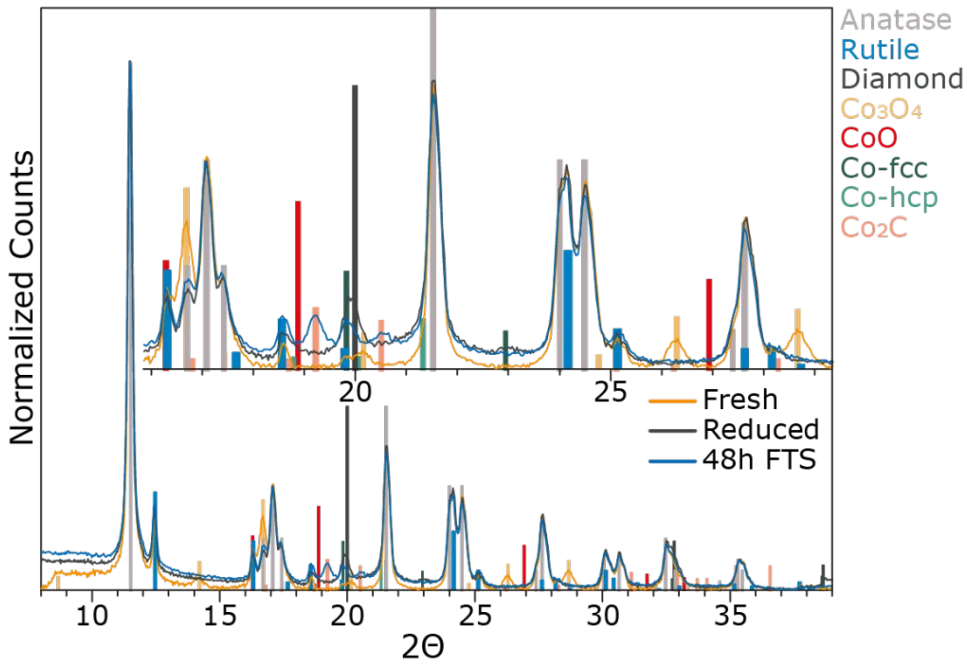

Figure S21. XRD patterns of the fresh Co/TiO_2 catalyst under study, and subsequently reduced and converted into the spent catalyst after approximately 2 days of FTS, along with lines indicating the diffraction peaks of different phases of Co that could be expected.

.

S5 Decarburization and Re-carburization

S5.1 Pressure and Temperature profile

After 48 h of FTS, the H_2/CO mixture was replaced by pure H_2 in order to decarburize the catalyst (still at 16 bar and 220 °C). After several hours the temperature was increased by 25 °C every hour until 300 °C and until a fully decarburized catalyst was obtained. Then, pure CO at 220 °C was flowed in order to carburize again until the beam time was over. The temperature

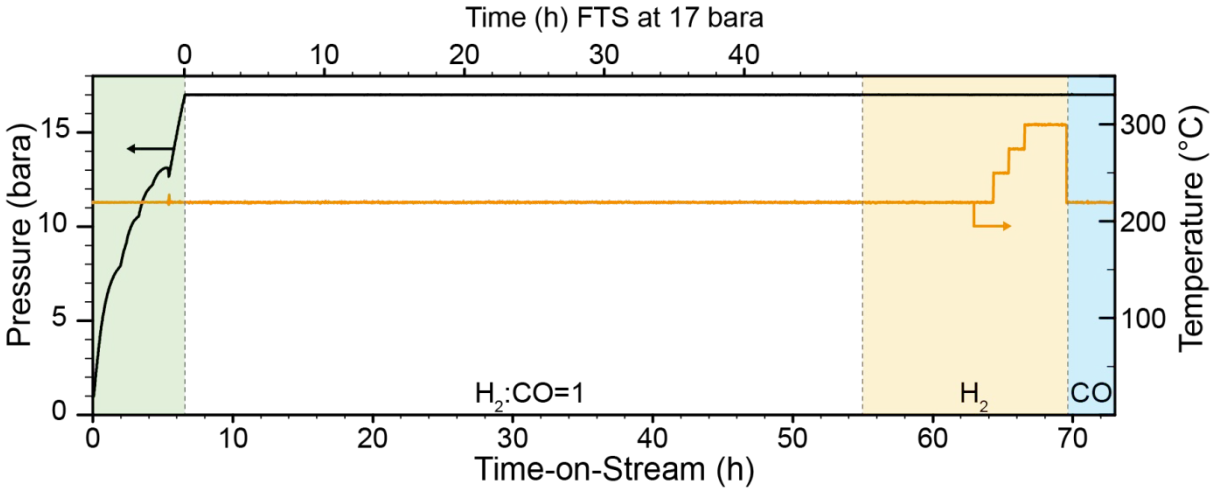

Figure S22. The reaction profile showing the decarburization in pure H_2 followed by carburization in pure CO.

and pressure profile of the whole experiment, including decarburization and re-carburization is shown in Figure S22.

S5.2 XANES during de- and re-carburization

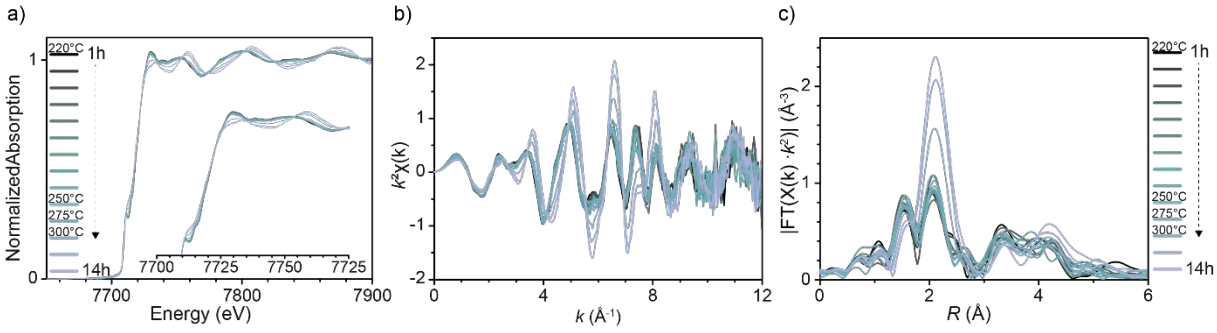

Figure S23. Co K-edge XANES spectra during the decarburization experiment in H_2 (a), and the

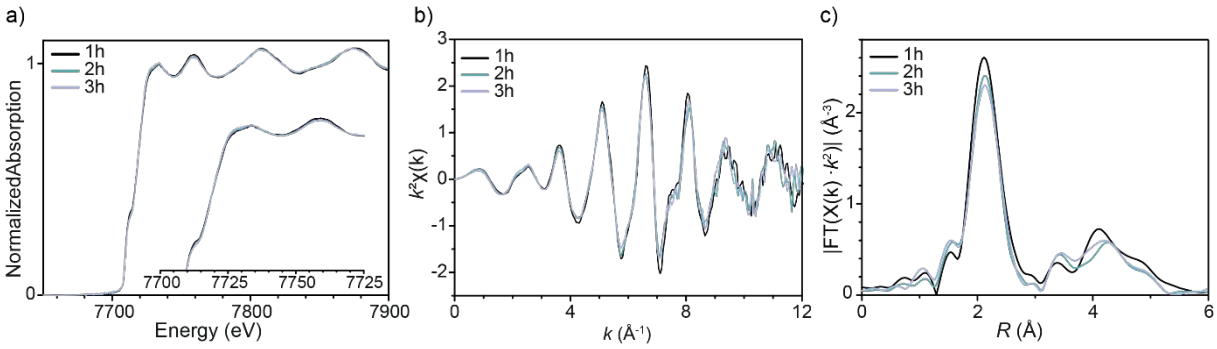

Figure S24. Co K-edge XANES spectra during the re-carburization experiment in CO (a), and the corresponding

S5.3 LCF of XANES during de- and re-carburization

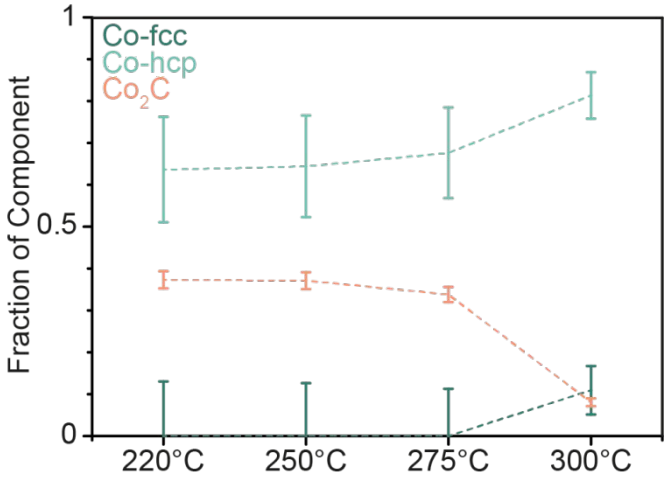

Figure S25. Linear combination fitting of the Co XANES during decarburization, spectra are merged per temperature. At 220 °C nothing is happening for about 8 hours. Raising towards 300 °C (with 25 °C·h^{-1}) shows a decarburization with at the end state: 81.3% Co-hcp, 10.9% Co-fcc and 8.1% Co_2C. The distinction between the two metallic cobalt is not definite as a nanoparticle effect plays a role here as well.

S5.4 Clustering over whole range

Clustering over the whole experimental range, including FTS, decarburization and re-carburization. The numbering in Figure S26d indicates the FTS (1-47h), decarburization at

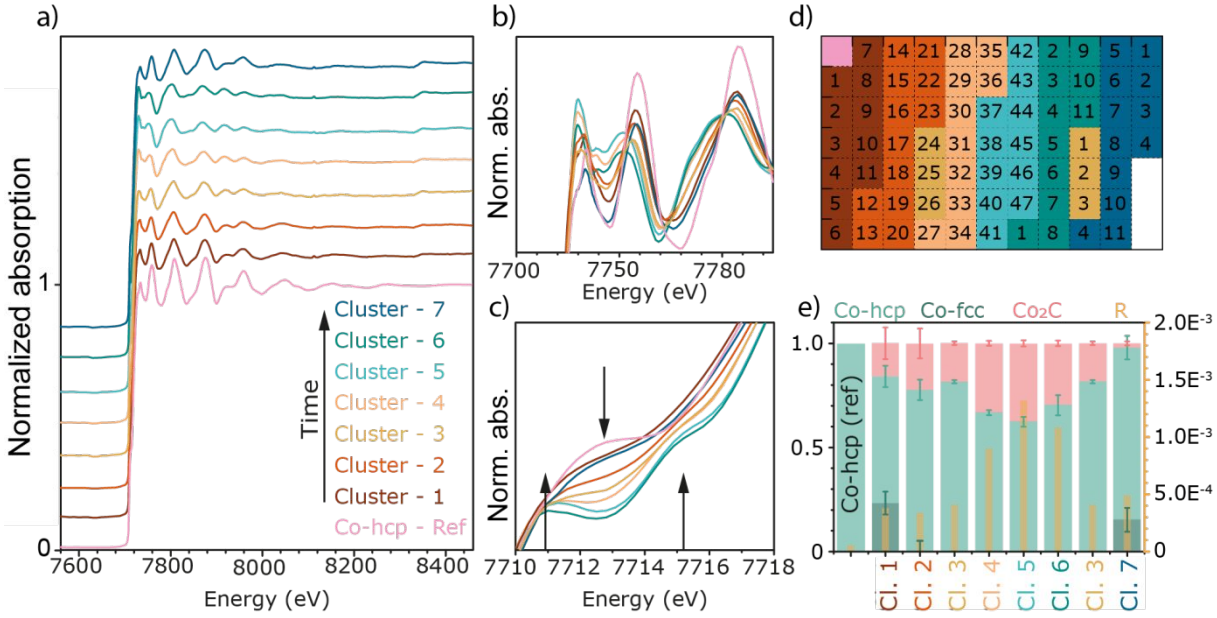

Figure S26. Principle component analysis and clustering of the *operando* XAS data shown in Figure 5 (clusters 1-5), plus the decarburization (clusters 6 and 7) after FTS. With this method, the large amount of spectra is downsized to 7 different clusters and a reference with time-on-stream (TOS) indicated in a) (offset for clarity). b-c) A zoom in of the areas with the most spectral changes. d) Shows the time frame of the different clusters with TOS. The colored boxes represent the cluster and the number the time in hours, with FTS until 47h, and starting at 1h from decarburization and raising temperature. The last 4 h represent the re-carburization trial. The different clusters were fitted with the reference spectra of Co-hcp, Co-fcc and Co_2C and the linear combination result is shown in e). With TOS the amount of Co_2C phase is increasing and metallic Co decreasing. The opposite holds for the decarburization.

220 ☐C (1-11h), decarburization with increasing temperature till 300 ☐C (1-11h) and the re-carburization (1-4h).

S5.5 Extra information on Cluster 3

As can be seen from Figure 5, 8 and S26, cluster 3 has a lower carbide average than cluster 2. This could be explained due to the decarburization we apply later on during the experiment.

Note that the following data is normalized and mean centered and therefore does not show an edge jump.

Cluster 3 consists of 6 spectra, three of them (24-26 h TOS) were recorded between cluster 2 or 4 and the other three between cluster 6 and 7 (see Figure S27a). The time periods of 24-26 h and 59-61 h are clearly visible in Figure S27b (red rectangles) due to the lack of spectral features. The less detectable features can be seen in Figure S27c/d (black and yellow line, respectively) compared to the surrounding clusters. This can be well explained by the fact that the features of clusters 2 and 4 and clusters 6 and 7 are almost perfectly anticorrelated. A mix of those 2 phases will flatten all features and this shows as a transition phase between a pair of clusters. It means the phase transition between these 2 clusters is much slower than our time resolution. It seems that spectra 24-26 are not exactly/purely a transition region, however, as they more closely resemble cluster 4 than 2. This is probably due to the sample realignment that was conducted in this time window (the hutch was entered to replace the CO detector necessitating a halt to collecting the XAS spectra). The signal was temporarily lost but recovered within those 3 hours (see Figure S28). The phase transition between hours 59-61 on the other hand is real and is made more visible in the score plots in Figure S28. The top graph shows the 3D score plot and the bottom the 2D with only PC1 and PC2. The numbers correspond to the hours TOS during the experiment and the colours correspond to the clusters assigned. The arrows indicate the time series in which spectra were recorded and were added to guide the eye. Cluster 3 (numbers 24-26 and 59-61) is manually “separated” by the striped lines nicely visualizing what happened. One can clearly see that the spectra recorded between 59-61h are a transition between the clusters 6 and 7 (green and dark blue, respectively) and that spectra 24-26h actually connect clusters 2 and 4 (orange and dark yellow, respectively) but have been clustered together with the spectra connecting clusters 6 and 7 because their

spectral features (or better, the absence of them) caused by the event that took place as described above, made them similar to the transition phase between clusters 6 and 7. This is an example for the challenges of long-term and high-pressure experiments and how careful data analysis can detect, isolate, and explain unforeseen events that might take place. If we had not done the clustering, we would also not have noticed this transition phase happening between 59-61h TOS.

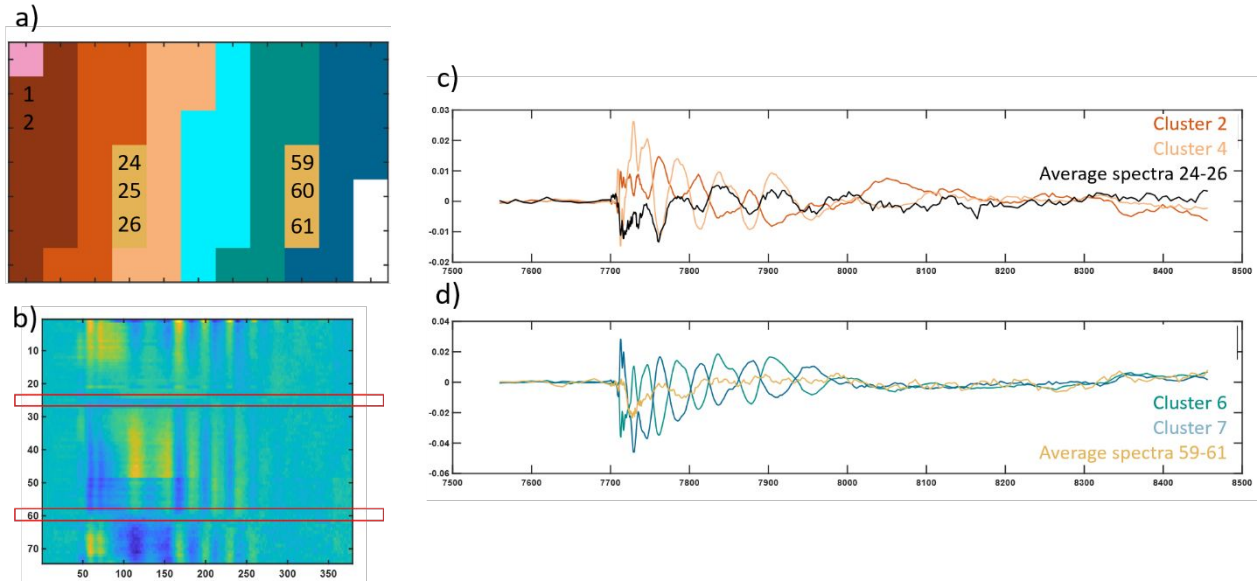

Figure S27. a) Indicates cluster 3 and the corresponding hours TOS. b) Shows the contour plot of all the spectra with TOS where the red rectangles indicate the times corresponding to cluster 3. As can be seen here, those appear to be almost featureless. This is made more visible in c) and d), where the average of the spectra 24-26h and 59-61h are plotted together with the clusters they connect.

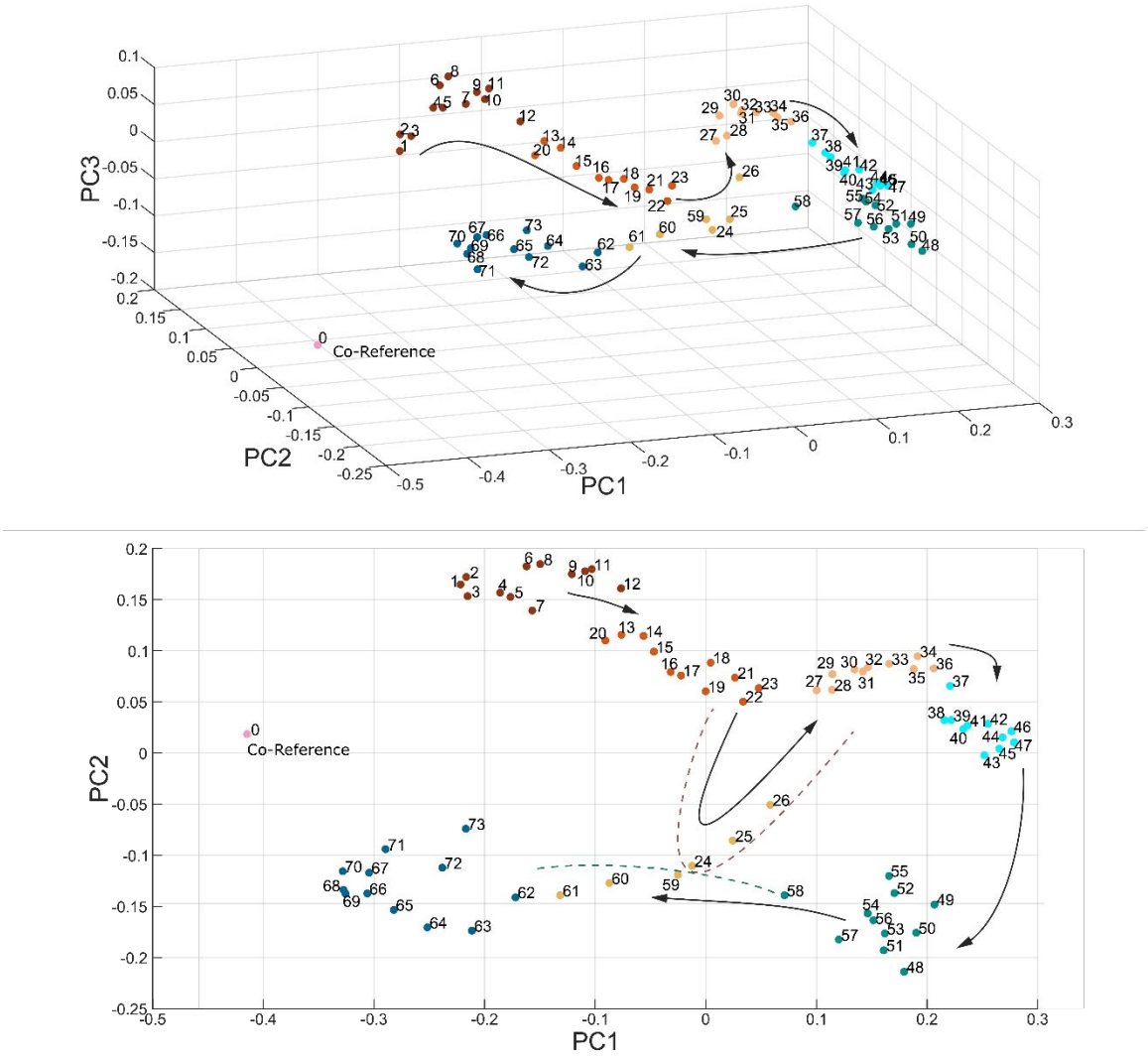

Figure S28. The top graph shows the 3D score plot and the bottom the 2D with only PC1 and PC2. The numbers correspond to the hours TOS during the experiment and the colours correspond to the clusters assigned. The arrows indicate the time series of the spectra, i.e. the order in which they were recorded during the experiment. The dashed lines in the bottom plot have been added manually to indicate the difference in time between those spectra (numbers 24-26 and 59-61). Here one can clearly see that the spectra of 59-61h are a transition between the clusters 6 and 7 (green and dark blue, respectively) and that spectra 24-26h should connect clusters 2 and 4 (orange and dark yellow, respectively), but due to the events that took place in this time period these spectra are almost featureless and have therefore been clustered together with the transition phase between clusters 6 and 7.

S6 Spent HAAFD-STEM-EDX mapping and XRD

S6.1 Spent images + histograms of sizes

Cobalt species had a wide size distribution ranging from sub-nm species up to 50 nm particles. Due to the low contrast, proper particle size analysis is not trivial. The analysis is blind to sub-nm species and does not include larger agglomerates (>5nm) that were seen

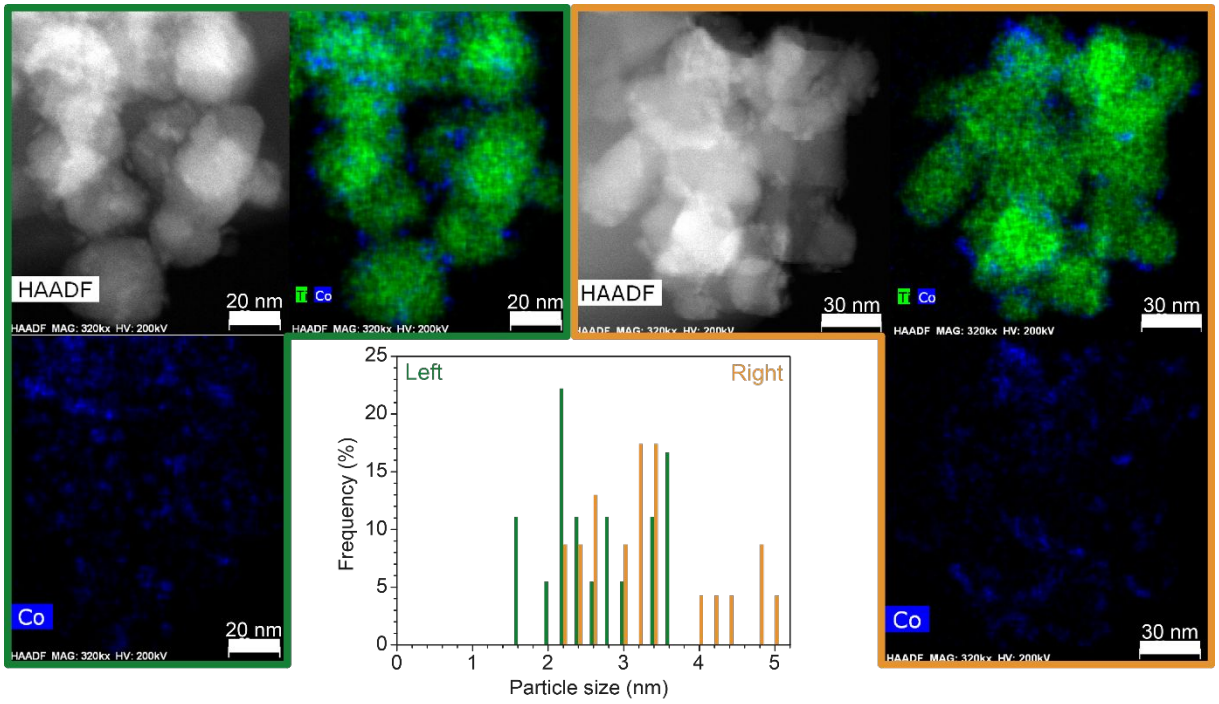

Figure S29. HAADF-STEM and EDX images of the spent catalyst including the Co particle size histograms taken from chemical maps of the spent catalyst after decarburization and re-carburization. Average size for the left is

elsewhere in the sample. Excluding sub-nm species and large agglomerates (>5 nm), the average particle size can be roughly estimated to be around 3 nm.

S6.2 Carbon mapping of spent exp-2

Carbon has mostly uniform distribution over the titania. Some Co particles exhibit enhanced concentration of coke, but not all metal particles display such high coke accumulation, as can be seen in Figure S30. Here, two regions are shown of which region one shows a cobalt particle

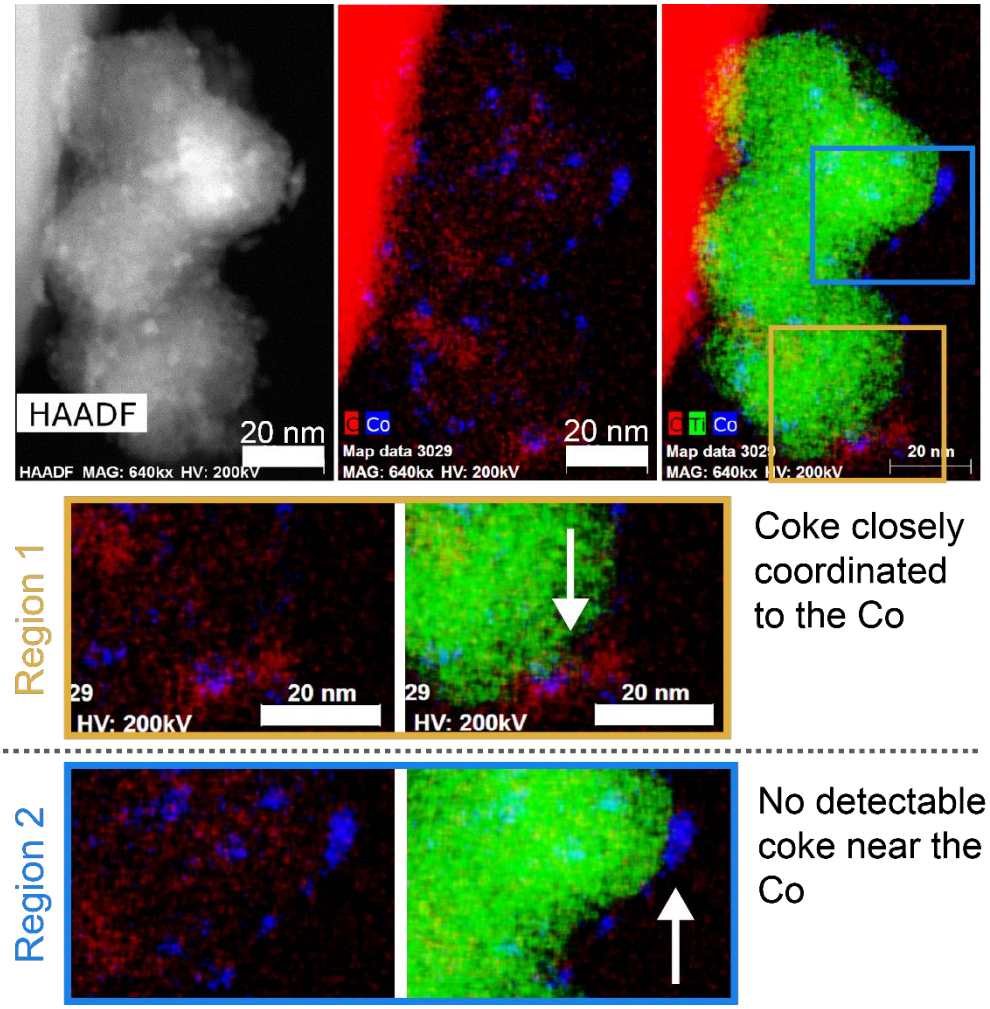

Figure S30. STEM-EDX maps showing regions of coke near the Co NPs (top). The dark red area in the top EDX maps is the carbon from the diamond dilution, cobalt is shown in blue and titania in green. The bottom images show the zoom in of the rectangles in the top right image.

with a high accumulation of carbon deposit and region 2 does not.

S6.3 XRD from spent XAS experiment-2

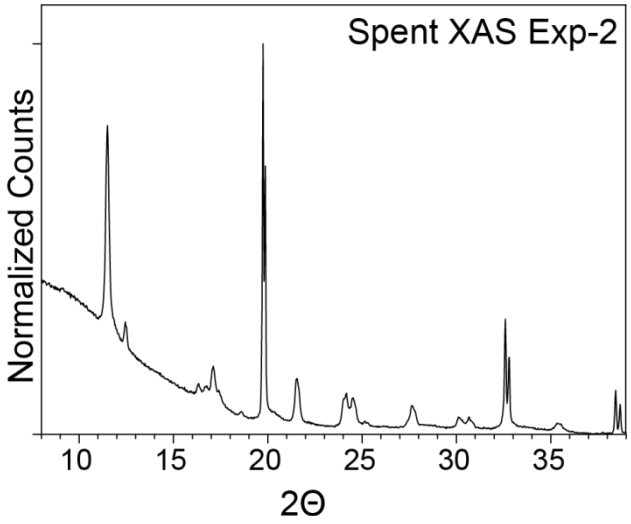

Figure S31. Diffractogram of the sealed spent sample after the second XAS experiment. Due to the diamond peak, the metallic cobalt is not visible. The broad band at lower 2Θ degrees could indicate small (<3 nm) particles.

S6.4 Spent of Exp-1

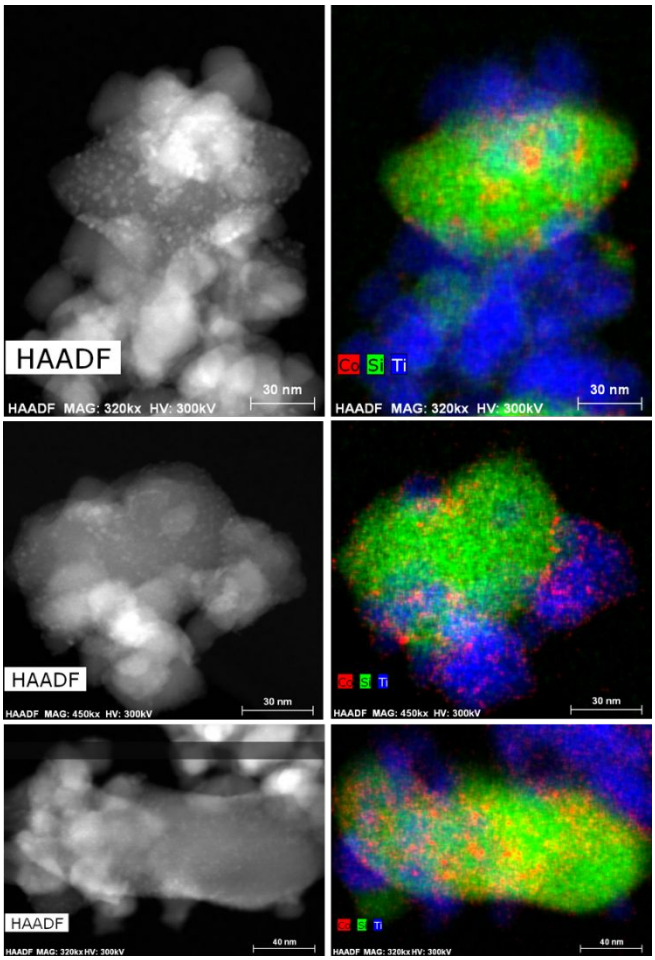

Figure S32. Spent 10 wt.% Co/TiO_2 diluted 1:2 with MCM-41 (SiO_2) by mass. On the left the HAADF images and on the right EDX chemical mapping, cobalt is shown in red, titania in blue and silica in green. Here cobalt migrated from the TiO_2 support to the SiO_2 diluent. An elemental analysis for the particle at the top is given in Figure 33

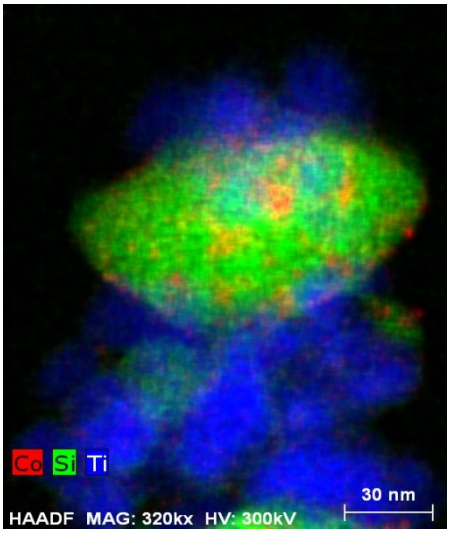

Element	Series	Net	Mass C (wt.%)	Norm. C. (wt.%)	Atom C. (at.%)	Error (1 σ) (wt.%)
Si	**K**	**106639**	**26.81**	**26.81**	**28.80**	**0.11**
Ti	**K**	**231982**	**67.33**	**67.33**	**57.16**	**2.05**
Co	**K**	**16291**	**5.86**	**5.86**	**4.04**	**0.21**
		Total	**100.0**	**100.00**	**100.00**	

Element	Series	Net	Mass C (wt.%)	Norm. C. (wt.%)	Atom C. (at.%)	Error (1 σ) (wt.%)
Si	K	79039	55.98	55.98	69.56	0.23
Ti	K	37612	32.00	32.00	23.32	1.00
Co	K	11338	12.02	12.02	7.12	0.41
		Total	100.0	100.00	100.00	

Element	Series	Net	Mass C (wt.%)	Norm. C. (wt.%)	Atom C. (at.%)	Error (1 σ) (wt.%)
Si	K	18396	8.96	8.96	14.43	0.09
Ti	K	157386	88.81	88.81	83.86	2.70
Co	K	3200	2.23	2.23	1.71	0.10
		Total	100.0	100.00	100.00	

Figure S33. Spent 10 wt.% Co/TiO_2 diluted 1:2 with MCM-41 (SiO_2) by mass. On the left the EDX chemical map, cobalt is shown in red, titania in blue and silica in green. Here cobalt has migrated from the TiO_2 support to the SiO_2 diluent. The elemental analysis of the different regions shows that the Si-rich region

(1) Hoffman, A. S.; Singh, J. A.; Bent, S. F.; Bare, S. R.; IUCr. In Situ Observation of Phase Changes of a Silica-Supported Cobalt Catalyst for the Fischer–Tropsch Process by the Development of a

Synchrotron-Compatible In Situ/Operando Powder X-Ray Diffraction Cell. *J. Synchrotron Radiat.* **2018**, *25*, 1673–1682.

(2) Singh, J. A.; Hoffman, A. S.; Schumann, J.; Boubnov, A.; Asundi, A. S.; Nathan, S. S.; Nørskov, J.; Bare, S. R.; Bent, S. F. Role of Co_2C in ZnO-Promoted Co Catalysts for Alcohol Synthesis from Syngas. *ChemCatChem* **2019**, *11*, 799–809.

(3) Liu, Y.; Wu, D.; Yu, F.; Yang, R.; Zhang, H.; Sun, F.; Zhong, L.; Jiang, Z. In Situ XAFS Study on the Formation Process of Cobalt Carbide by Fischer-Tropsch Reaction. *Phys. Chem. Chem. Phys.* **2019**, *21*, 10791–10797.

(4) Kwak, G.; Woo, M. H.; Kang, S. C.; Park, H. G.; Lee, Y. J.; Jun, K. W.; Ha, K. S. In Situ Monitoring during the Transition of Cobalt Carbide to Metal State and Its Application as Fischer-Tropsch Catalyst in Slurry Phase. *J. Catal.* **2013**, *307*, 27–36.

(5) Mohandas, J. C.; Gnanamani, M. K.; Jacobs, G.; Ma, W.; Ji, Y.; Khalid, S.; Davis, B. H. Fischer-Tropsch Synthesis: Characterization and Reaction Testing of Cobalt Carbide. *ACS Catal.* **2011**, *1*, 1581–1588.